ISSN 1054-660X, Laser Physics, 2006, Vol. 16, No. 5, pp. 765–773.
© MAIK "Nauka/Interperiodica" (Russia), 2006.
Original Text © Astro, Ltd., 2006.

Experimental Results for Propagation of Diffuse Photon-Density Waves up to 1 GHz in a Tissue-Like Medium Containing an Absorbing Edge

U. J. Netz[a], A. H. Hielscher[b], A. K. Scheel[c], and J. Beuthan[a]

[a] *Department of Medical Physics and Laser Medicine, Charité–Universitätsmedizin Berlin, Fabeckstrasse 60-62, Berlin, 14195 Germany*

[b] *Departments of Biomedical Engineering and Radiology, Columbia University, ET351 Mudd Building, MC 8904, 500 West 120th Street, New York, NY 10027 USA*

[c] *Department of Medicine, Nephrology and Rheumatology, Georg-August-University Göttingen Robert-Koch-Strasse 40, 37075 Göttingen, Germany*

e-mail: uwe.netz@charite.de

Received December 26, 2005

Abstract—Optical imaging in the near-infrared (NIR) region provides the possibility to detect and determine pathological changes in human tissue without the drawback of ionizing radiation and with little technical and financial effort. Especially in rheumatoid arthritis, imaging by optical tomography to detect early inflammations in joints has the potential to become a supportive tool to common imaging modalities. One way to enhance the resolution and specificity of optical tissue characterization is to use the frequency domain instead of DC intensity measurement. Intensity modulation of a light source leads to propagation of diffuse photon-density waves (PDW) through the tissue. In this study, we report basic experimental results on tissuelike phantoms to determine the optimal parameters for PDW-transillumination of finger joints. We used PDW with modulation frequencies from 100 MHz up to 1 GHz to scan across a tissuelike phantom containing an absorbing plane bounded by an edge. The geometrical extents of the phantoms are similar to human finger joints. We measure the transmitted PDW and show that amplitude and phase behaves at the edge as expected according to theoretical predictions. An increasing modulation frequency leads to increasing slope of the amplitude decay at the edge but decreasing signal-to-noise ratio. Even at 1 GHz, the edge is detectable.

PACS numbers: 87.57.Ce, 87.63.Lk, 87.64.Cc, 87.66.Xa

DOI: 10.1134/S1054660X06050069

INTRODUCTION

The purpose of studying the optical transillumination of tissue has always been to find alternatives to existing methods of tissue characterization, some of them invasive ones, and to extend the range of diagnostic possibilities. The measurement of optical signals in the ultraviolet (UV) to infrared (IR) wavelength domain is characterized by high tissue scattering of light, limiting the resolving power and the contrast of the images generated. Absorption in the near IR is particularly low, rendering optical transillumination of tissue up to several centimeters in depth possible. So, optical transillumination can be advantageously applied, especially when information will be obtained from low depths or small geometries.

Inflammatory changes (i.e., synovial proliferation) in finger joints affected by rheumatoid arthritis offer a good possibility to obtain information on the state of the joint by light transmission measurements [1–5]. Using a diaphanoscopic method, it was possible to demonstrate in the first clinical results that the inflammation stage can be evaluated [6, 7]. Representing the optical properties in a joint using an optical tomographic imaging process in comparison with an ultrasonic imaging process, it was also possible to correctly evaluate the inflammation stage in primary diagnostics [8–10]. Despite the high photon scattering in the volume of the finger joint, a spatial resolution which would be sufficient for functional imaging can be obtained by optimization of the imaging process.

The transmission of intensity-modulated light through diffusely scattering tissue can be described as propagation of a photon-density wave (PDW) through the tissue [11]. For a tomographic reconstruction the detection of phase and modulation (amplitude) of the waves delivers more information than a simple intensity measurement. Therefore, transillumination by means of a PDW is likely to improve both the detection of small differences in the optical properties and the specification of symptoms [12, 13].

Theoretical calculations and simulations were made to determine the resolving power of the PDW-based transillumination of tissue, and the results of experiments on phantoms were published relating to the detectability and characterization of inhomogeneities or of the edge spread function [14–18]. It turned out that the resolution generally increases with rising frequency, which is mostly due to the increasing phase

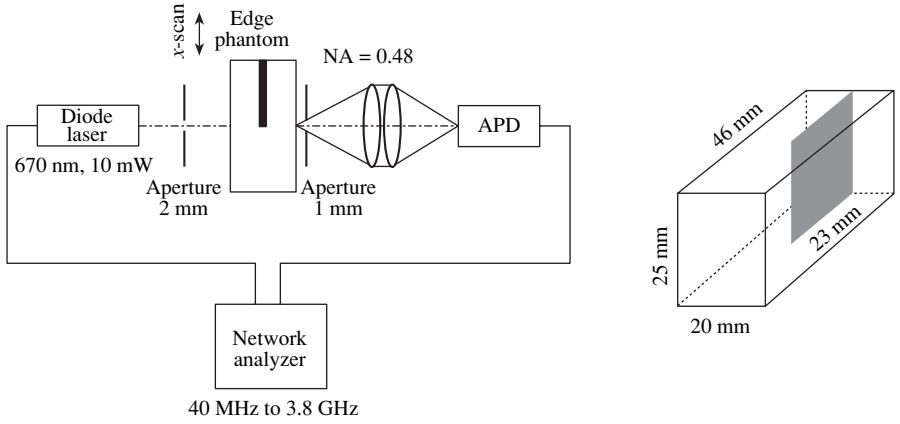

Fig. 1. Experimental setup and phantom geometry for scanning amplitude and phase measurement.

shift at higher frequencies. However, the noise, as given by the standard deviation in the amplitude and phase measurements, also increases with increasing frequency. Therefore, an optimum modulation frequency for maximum resolution and contrast usually exists. This optimum frequency may differ depending on the tissue and the transillumination geometry, as for example shown by Boas et al. [14] in simulations studies and by Toronov et al. [20] in simulations and experimental studies.

As far as we know, basic experimental investigations on the resolution or SNR in the frequency domain have been made only up to a few hundreds of megahertz. Investigations extending into the gigahertz domain were made via technically more complicated measurements in the time domain and subsequent Fourier transformation [19, 20]. However, this approach does not take into account the particular noise sources in frequency-domain measurements.

Our experiments presented in this paper were aimed at investigating the extent to which the signal and noise depend on the modulation frequency when a frequency-domain measuring setup is used for imaging small geometries, as encountered for example in finger imaging, and whether the PDW can be reasonably utilized in practice up to 1 GHz. For this purpose, investigations covering a frequency domain from 100 MHz to 1 GHz were made on a phantom with an absorbing edge.

METHODS

The propagation of the photon density as a wave in a homogeneous, infinite medium can be described by means of the diffusion approximation to the radiative transfer equation [15, 21].

It can be represented as an equation which is composed of a DC and an AC portion, i.e.,

$$U = U_{DC} + U_{AC}\exp[i(kr - \omega t) - r\mu_{AC}], \qquad (1)$$

with the first term on the right-hand side of (1) being the time-independent DC part and the second term being the time-dependent AC part of the wave. $U_{AC}\exp(-r\mu_{AC})$ is the amplitude of the AC part, μ_{AC} is an effective AC attenuation coefficient, k is the wave vector, r is the path covered between the source and the detector, and $\omega = 2\pi f$ is the modulation angular frequency. μ_{AC} and k depend primarily on the optical properties, i.e., absorption and scattering, of the medium and the frequency.

The optical properties of scattering media are described by the scattering coefficient μ_s, the absorption coefficient μ_a, and the anisotropy factor g. The anisotropy factor is a characteristic value for the probability distribution of the scattering direction with a range of [–1, 1]. With typical values of 0.9, human tissue is primarily forward-scattering.

However, there is no longer differentiation by scattering direction in the diffusion approximation. Employing the reduced scattering coefficient $\mu_s' = \mu_s(1 - g)$, an isotropic scattering is supposed instead. In order to be able to apply this type of diffusion approximation, the scattering must clearly dominate the absorption [15, 21]. The thickness of the transilluminated medium and the distance between the source and the detector should be larger than the medium free path length $1/\mu_s'$ respectively.

Experimental Setup

The core of the experimental setup is a vector network analyzer (Advantest Corporation R3765AH, Tokyo, Japan) that serves as modulation source and provides signal analysis (Fig. 1). Furthermore, the setup contains an optical system comprising a diode laser and a detector system for modulated light transmission measurement, a stepping motor unit, and digital data acquisition by a computer.

The vector network analyzer is used to generate and analyze RF signals from 100 MHz up to 1 GHz. RF out-

put of the network analyzer is directly put into the modulation entrance of the diode laser operating at wavelength 670 nm (LISA laser products OHG, Katlenburg-Lindau, Germany). The modulation power is set to 5 dBm. The collimated beam is restricted by an aperture to a beam diameter of 2 mm and is attenuated by neutral density filters to restrict the intensity to suitable values for the applied detector. A 1-mm entrance aperture is imaged to the detector by a lens system with a numerical aperture of 0.48. The detector is an avalanche photo diode (APD) (Hamamatsu C5658), covering a frequency range from 1 MHz to 1 GHz for measurement of AC modulation, directly connected to the analyzer. The bandwidth of analyses is set to 10 Hz. Another APD (Hamamatsu C5460-01) is used for measurement of the DC light transmission and is connected to an oscilloscope. The laser and detector systems are both mounted on a stepping motor translation stage for coaxial scanning across the phantom surface. A computer connected via a GPIB bus system serves to control the network analyzer and the stepping motor unit.

Phantom

The phantom, which was provided by the Physikalische Technische Bundesanstalt, Berlin, Germany [22], is made of epoxy resin, homogeneously distributed fused silica spheres ($r = 255$ nm) as scattering particles, and an additional dye. The optical properties of the phantom, i.e., absorption coefficient and reduced scattering coefficient, were determined with a double integrating sphere measurement system [23]. We found the absorption and scattering coefficient to be $\mu_a = 0.013$ mm^{-1} and $\mu_s' = 2$ mm^{-1}, respectively. A blackened 1-mm aluminium sheet was inserted in a tight slit in the xy plane at $z = 10$ mm to generate a highly absorbing sharp edge (Fig. 1). The edge is located in the middle of the phantom at $x = 23$ mm. Scanning is provided in the x direction. A second phantom without an edge but with identical optical properties was used for reference measurement.

Calibration

The network analyzer puts the signal at the input internally in reference to the modulation at the output. The amplitude A relatively to the modulation power at the output and the relative phase Φ in the range $[-\pi, \pi]$ are measured. In addition to the transmission characteristic of the transilluminated phantom, these measured values also contain the attenuation and phase shift of the optical and electrical system, i.e.,

$$\begin{aligned} \Phi_{\text{measured}} &= \Phi_{\text{phantom}} + \Phi_{\text{system}}, \\ A_{\text{measured}} &= A_{\text{phantom}} \cdot A_{\text{system}}. \end{aligned} \tag{2}$$

To determine only the phase shift and the relative amplitude attenuation caused by the phantom, the transmission behavior of the system is to be determined as a calibration in the first step. For this purpose, the light is attenuated by a neutral density filter instead of the phantom. Since the filter contribution to the phase shift is negligible, the measured phase is equal to the phase shift generated by the system. The amplitude is attenuated by the filter to the same extent as the DC proportion, independent of the modulation frequency. The amplitude spectrum after the filter thus reflects the system part of the AC attenuation multiplied by the filter transmission.

Measurement

Prior to each measurement, the system's dark signal was measured with the laser diode covered. For the calibration measurement, a combination of two filters was used, which jointly featured a transmission of 3.6×10^{-4} at 670 nm. The calibration for the DC transmission was also measured using these two filters. The laser and the detector system were coaxially scanned over the phantom in 1-mm increments in the x direction at half the y height. At each position, the laser was modulated over a frequency range from 100 MHz to 1 GHz and in increments of 50 MHz amplitude and phase were determined. The measurements of dark signal, calibration, and the complete scanning of the phantom were repeated 10 times each, in order to reduce the statistic signal variations by forming a mean value. The DC transmission is determined at the oscilloscope. Scanning is started in the x direction 2 mm from the phantom boundary.

Analyses

Amplitude and phase variations are caused by statistical changes in the light generation and modulation (photon noise) and in the detection (shot noise, thermal noise) due to positioning errors and to the signal analysis of the network analyser. These variations can be reduced by statistic averaging. Only the total error is considered here.

The dark signal according to (1) is deducted from all measurements:

$$U_k = U - U_D. \tag{3}$$

The calibration phase is deducted from the measured phase and the amplitude measured is divided by the calibration amplitude. After that, the phase is corrected by 2π at phase jumps so that there is a constant phase course. The total amplitude and phase uncertainty thus consists of the dark signal, the measurements, and the calibration.

The demodulation $MD = AC/DC$ is also measured and demonstrates how differently the AC amplitude is attenuated compared with the DC intensity.

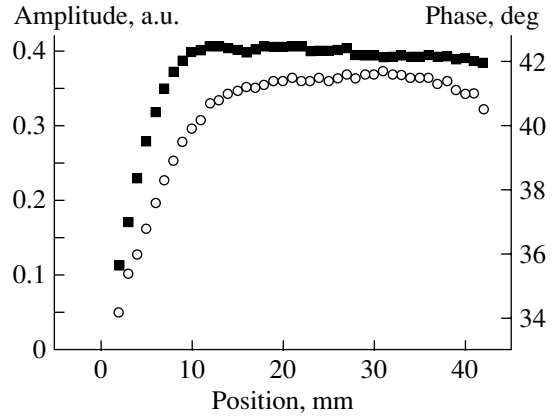

Fig. 2. Amplitude (■) and phase (○) scan across the homogeneous phantom at 100 MHz modulation frequency, scan starts 2 mm inside from phantom boundary.

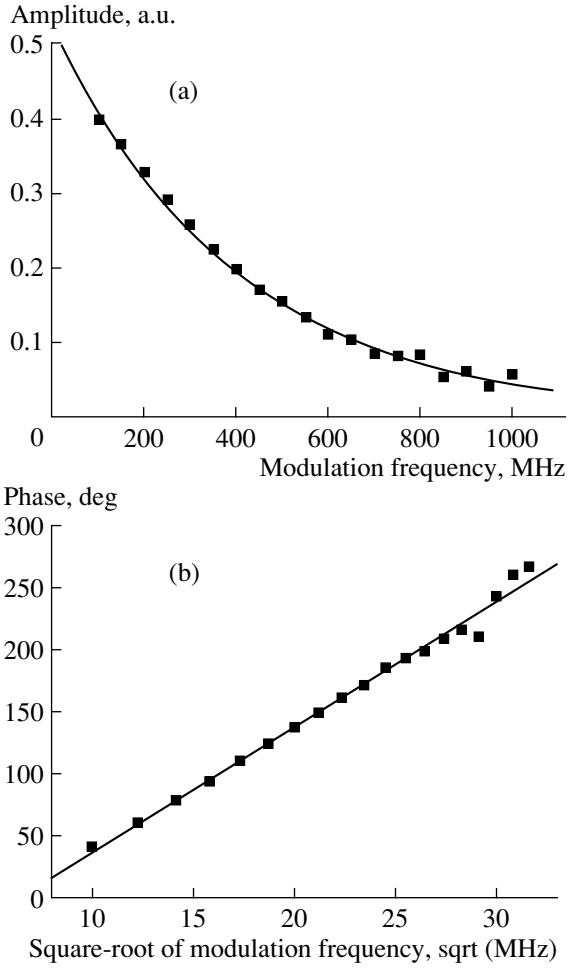

Fig. 3. (a) Amplitude and (b) phase in the middle of the homogeneous phantom vs. modulation frequency and square-root of modulation frequency, respectively, with exponential and linear regression, respectively.

To evaluate the signal quality, the signal-to-noise ratio of the measured data was calculated. The SNR of the amplitude is defined as

$$\mathrm{SNR} = \frac{A_{\mathrm{signal}}}{\sigma_A}, \tag{4}$$

i.e., through A and not through A^2, because, contrary to electromagnetic waves, the PDW's amplitude A as such is proportional to the energy. The standard deviation, σ_A, of the amplitude is calculated through the repeated measurements. The SNR for the phase is defined in the same fashion. However, this definition is to be considered cautiously. The phase cannot be measured as an absolute value, but only in the range of $[-\pi, \pi]$. Although it is possible to subsequently correct the phase in a range exceeding $[-\pi, \pi]$ at phase jumps in the frequency spectrum or in the spatial course because it mostly behaves constantly, it is still not known when measuring if the absolute phase is already n times 2π higher. Therefore, the phase variation can never be measured in a range exceeding $[-\pi, \pi]$.

RESULTS

Dark Signal

The dark signal reflects the frequency response of the complete system without light. The phase is affected by noise over the total range of $[-\pi, \pi]$. The amplitude increases slightly towards 1 GHz; the phase jitter diminishes a little.

Homogeneous Phantom

Due to the finite extent of the phantom, which was selected to be fingerlike in the y and x directions, the influence of the boundaries has to be initially investigated. In the x direction, the DC signal, amplitude, and phase shift increase towards the middle of the phantom. In the DC signal and in the amplitude, the influence of the phantom boundary vanishes within the measuring error after approximately 10 mm and in the phase after approximately 13 mm (Fig. 2). The depth at which the boundaries are still of influence becomes lower towards higher frequencies.

The frequency behavior of amplitude and phase is represented in Figs. 3a and 3b. With increasing modulation frequency, the amplitude drops almost exponentially, while the phase increases approximately linearly with the root of the modulation frequency. This is to be expected according to the diffusion approximation [15]. At the boundary and in the middle of the phantom, neither the signal nor the variations show characteristic differences in their frequency behavior.

Edge Phantom

The edge phantom consists of the same material as the homogeneous phantom. Far from the edge, the two

phantoms show the same transmission properties. Towards the edge, the amplitude starts getting smaller and drops behind the edge (Fig. 4a). On the spot where the source and the detector are exactly in line with the edge, the amplitude is already less than half its original size. With the frequency increasing, the amplitude regression starts closer to the edge and proceeds over a shorter distance, which means that it is steeper (Figs. 5a and 6). At high frequencies, the signal before the edge is also slightly higher than the dark signal; thus, the amplitude contrast is decreasing (Fig. 8).

While the phase gets smaller close to the edge, it quickly rises behind it (Fig. 4b). The minimum is one or two millimeters before the edge. With the frequency increasing, the phase shows a more distinct minimum and a steeper increase behind the edge (Fig. 5b). From approximately 700 MHz, this course is hardly recognizable because of the increased noise and is therefore no longer represented in Fig. 5b.

The normalized demodulation MD represented in Fig. 7 shows the difference between the DC and the AC parts. Close to the edge, it increases with the frequency.

Signal-to-Noise Ratio

The noise of the amplitude on the homogeneous phantom is almost constant and increases slightly over the frequency spectrum (Fig. 9a). The noise of the phase increases approximately exponentially to the square root of the frequency (Fig. 9b). The SNR of both amplitude and phase steeply slopes with the modulation frequencies larger than 250 MHz (Figs. 9c and 9d). At approximately 150–200 MHz, a maximum in the SNR can be observed, both in amplitude and phase. This maximum occurs both at the homogeneous phantom and at the edge and is independent of position. Towards the edge, the SNR slowly falls off due to the fading signal and comes more or less close to the dark signal behind the edge (not represented).

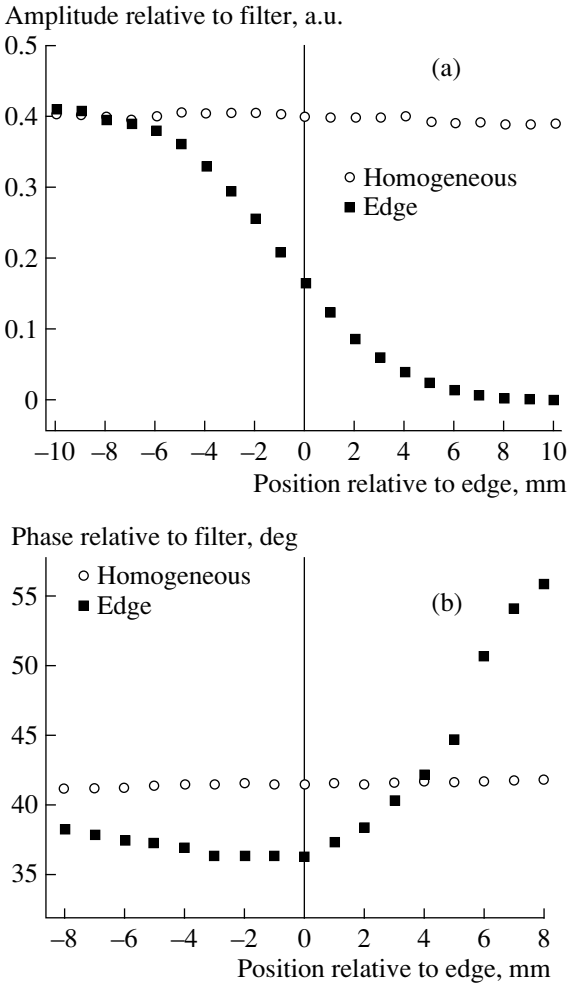

Fig. 4. Edge phantom: (a) amplitude and (b) phase at 100 MHz compared to homogeneous phantom in reference to neutral density filter.

DISCUSSION

In the dark signal, the signal variations diminish at high frequencies, while the amplitude slightly increases. Real signals seem to develop, which should be a systematic error. This error is caused by the modulation input of the laser acting more and more as an antenna with the frequency increasing. Therefore, the detection system is subjected to electromagnetic interference by the RF signal.

The increase in the phase shift with increasing modulation frequency and the decrease of the amplitude with increasing modulation frequency qualitatively show the behavior to be expected according to the diffusion approximation [15]. The effect on the boundary and the edge can be described by the diffuse photon paths. The regression of both amplitude and phase towards the boundary of the phantom (Fig. 2) can be explained by an increasing probability for the scattered photons to laterally leave the phantom. This means that only a few scattered photons finally do reach the detector. Therefore, the phase as a measure for the medium pathway of the photons must be smaller, and the DC and AC parts decrease.

Since the upper and the lower boundaries of the phantom in the y direction have the same influence on the light propagation when scanning, the phase for a phantom height of 25 mm may be systematically somewhat smaller due to lateral losses, as if the phantom had an infinite lateral extension.

As far as the transillumination of finger joints is concerned, distinct losses are to be expected, as the extension is even smaller. This influence, however, should decrease towards higher frequencies. Also, the absorption coefficient for clinical finger measurements should be rather higher than that set in the phantoms used here. This would reduce the influence of the boundaries.

On the level of the edge, the diffuse photon paths in the medium lead to an attenuation of the amplitude by

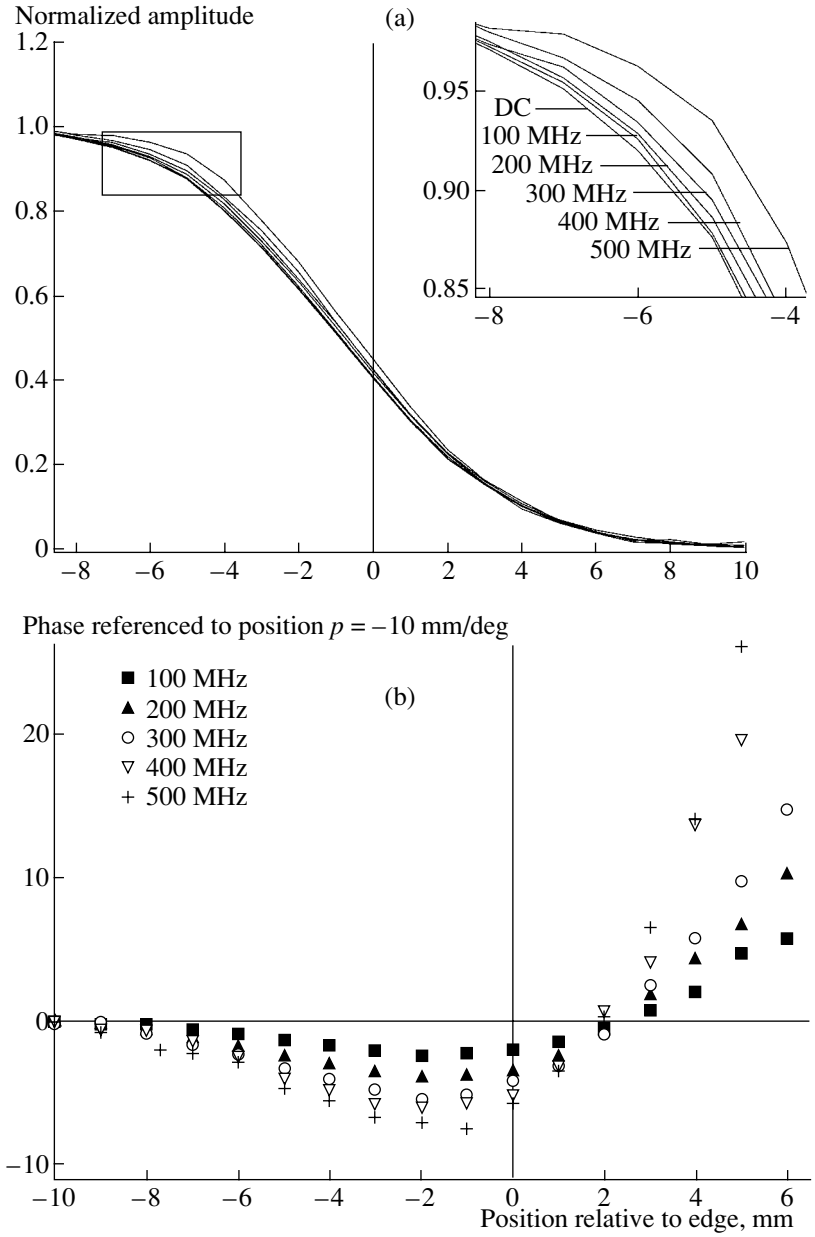

Fig. 5. (a) Normalized amplitude at the edge phantom compared to homogeneous. Connecting lines are used only for better illustration. (b) Phase at the edge phantom compared to homogeneous; each curve is normalized to its value at position $x = -10$ mm.

more than half (Fig. 4a). The closer to the edge one gets, the more photons are absorbed which, on their way to the detector, would have passed the level of the edge several times, thus, e.g., hitting the edge after having passed from the reverse side. With the frequency increasing, the amplitude regresses more steeply on the edge (Fig. 5a). If we suppose the PDW going through the scattering medium was a wave composed of many individual ones which are generated in each scattering event, according to Huygen's principle, all parts traveling a longer distance are attenuated more strongly because of the attenuation with $\exp(-r\mu_{AC})/r$ [15]. Since the effective attenuation coefficient μ_{AC} rises with the frequency, to an increasing extent, only parts which propagate through the medium by the shortest route are detected. At the same time, the medium path length decreases. Due to this, the phase gets smaller near the edge (Fig. 5b). Behind the edge, the mean path length ascends drastically, and the phase increases.

The demodulation *MD* in Fig. 7 demonstrates after normalization that the DC transmission falls off quicker in relation to the AC part on the edge and that this difference becomes larger with the modulation frequency. The larger the demodulation on the edge, the later the AC amplitude starts regressing.

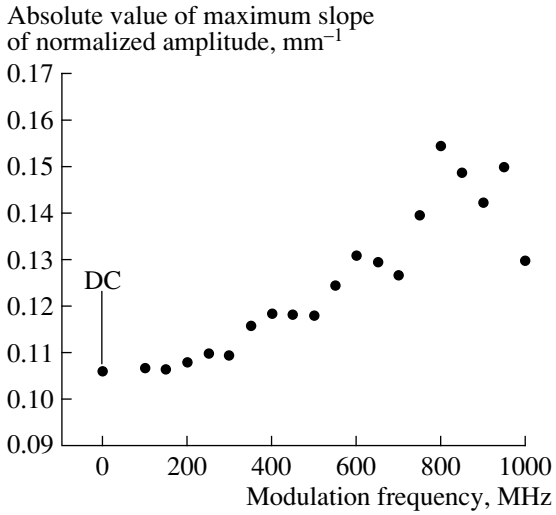

Fig. 6. Absolute value of maximum of the slope of the normalized amplitude at the edge.

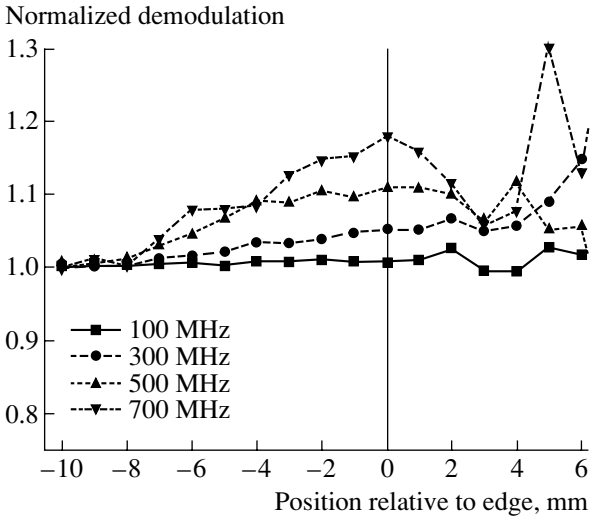

Fig. 7. Normalized demodulation (AC/DC) at the edge.

Referring to the noise, Toronov et al. analytically derived for pure shot noise that the phase variations rise proportionally to 1/AC and that the amplitude noise occurs independently of the frequency [20]. Boas et al. supposed in their theoretical considerations on the detection and characterization of inhomogeneities that the main sources of noise are shot noise and inaccuracies in the source and detector positions [14]. Considering changes in amplitude and phase due to perturbation by spherical scattering or absorbing inhomogeneities, they conclude that the amplitude noise caused by shot noise should rise circa exponentially with the root from the frequency, while the positioning-error related noise increases circa linearly with the square root of the frequency. In the phase the shot, noise rises exponentially with the frequency, while the noise due to positioning inaccuracies increases linearly with the square root of the frequency.

In our experiments, the amplitude noise is almost independent of the frequency (Fig. 9a). The phase noise increases less sharply than in the theoretical models, about exponentially with the square root of the frequency (Fig. 9b). Thus, our experiments correspond to the results of Toronov et al. Considering the SNR, Toronov et al. investigated changes due to absorbing inhomogeneities in the human brain by Monte Carlo simulation. They found a maximum in the phase SNR between 300 to 500 MHz. According to Boas et al., who looked at photon-density waves in a 6-cm-thick slab, SNR regresses steadily to high frequencies. During detection of scattering inhomogeneities, however, the phase SNR reaches its maximum at about 500 MHz. The amplitude SNR falls off steadily. In our experiments, we determined a maximum around 200 MHz, which is most likely due to different phantom geometries and optical properties. This discrepancy has to be further investigated.

CONCLUSIONS AND OUTLOOK

The experiments referring to the PDW transillumination of a tissuelike phantom with an absorbent edge qualitatively showed a signal course along the edge and a signal dependence on the modulation frequency that had been predicted in theoretical investigations.

After climbing to a maximum at 150–200 MHz, the SNR regresses with the frequency, more quickly in the amplitude than in the phase. Even at 1 GHz, the edge can still be represented in the amplitude with a sufficient SNR. Due to the strong phase noise increase, the edge in the phase was clearly recognizable only to approximately 700 MHz. Because a limited geometry

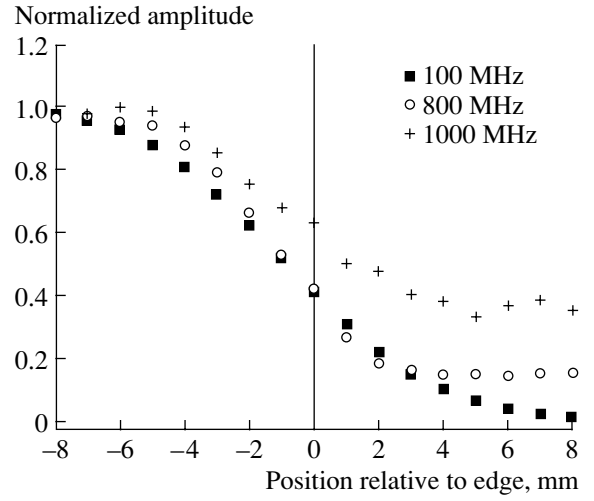

Fig. 8. Normalized amplitude across the edge for high frequencies compared to 100 MHz.

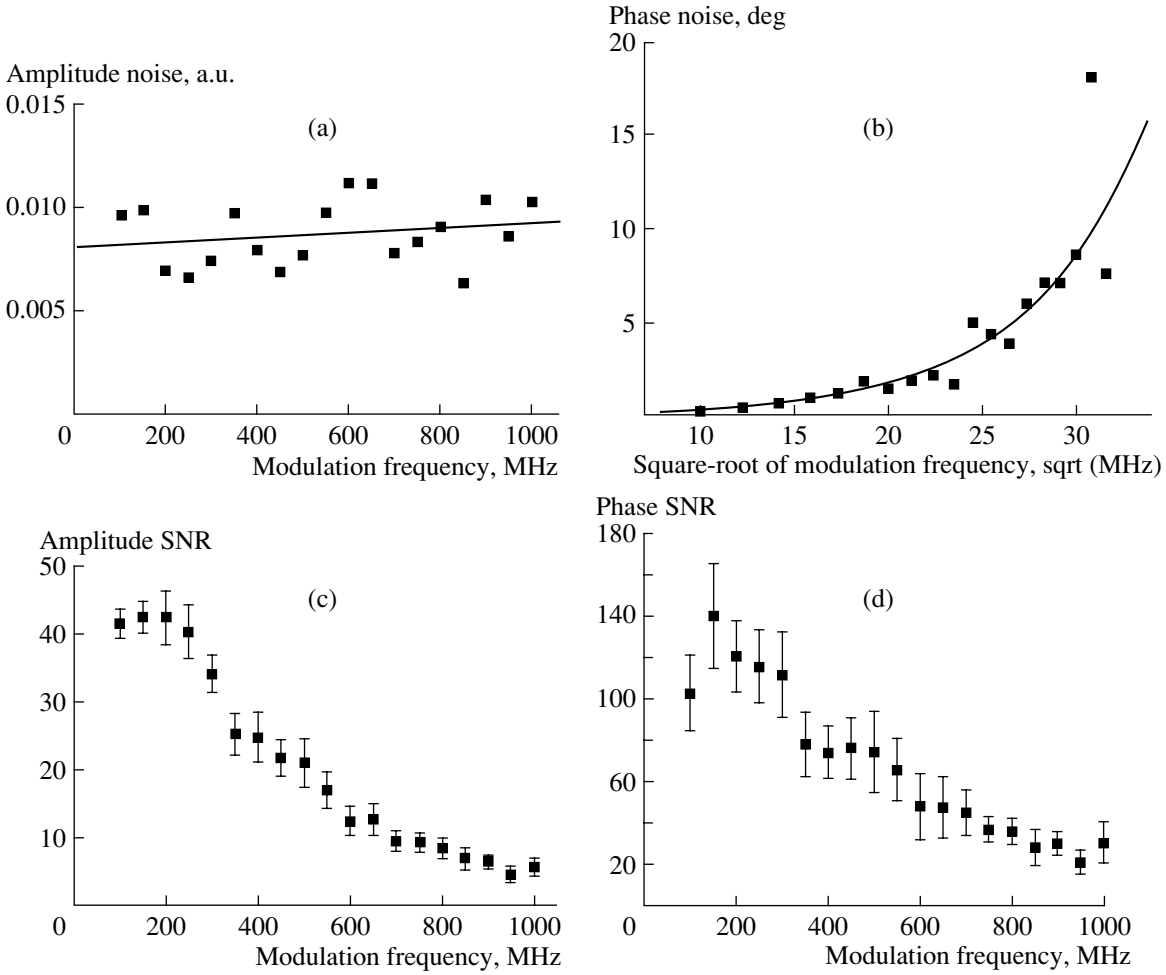

Fig. 9. (a) Amplitude noise and (b) phase noise in the middle of the homogeneous phantom ($x = 23$ mm) with linear and exponential regression, respectively, (c) amplitude signal-to-noise ratio and (d) phase signal-to-noise ratio for the homogeneous phantom, mean and standard deviations over 20 x positions.

had been selected for the phantom used, the signal was slightly influenced by the boundaries.

The results lead to the conclusion that, due to the small geometric dimensions of finger joints, transillumination using PDW up to and in excess of 500 MHz seems reasonable despite the high attenuation. The availability of additional data compared to conventional intensity measurements should decisively improve the tomographic reconstruction of the optical properties in joints. A detailed analysis of how sensitively a frequency domain reconstruction method responds to spatial changes of the optical properties should be made with a finger phantom reflecting in more detail the anatomical structure and which permits the optical parameters to be specifically varied.

ACKNOWLEDGMENTS

This work was supported by the grant R01 AR46255 from the National Institute of Arthritis and Musculoskeletal and Skin Diseases (NIAMS), United States, which is part of the National Institutes of Health.

REFERENCES

1. J. Beuthan, O. Minet, G. Müller, and V. Prapavat, in *Medical Optical Tomography: Functional Imaging and Monitoring*, Ed. by G. Müller, B. Chance, R. Alfano, et al. (SPIE, Bellingham, Washington, 1993), p. 263.
2. V. Prapavat, W. Runge, A. Krause, et al., Minim. Invasive Med. **8** (1–2), 7 (1997).
3. Y. Xu, N. Iftimia, H. Jiang, et al., Opt. Express **8**, 447 (2001).
4. J. Beuthan, U. Netz, O. Minet, et al., Quantum Electron. **32** (11), 945 (2002).
5. Y. Xu, N. Iftimia, H. Jiang, et al., J. Biomed. Opt. **7**, 88 (2002).
6. A. K. Scheel, A. Krause, I. Mesecke-von Rheinbaben, et al., Arthritis Rheum. **46**, 1177 (2002).
7. A. Schwaighofer, V. Tresp, P. Mayer, et al., IEEE Trans. Biomed. Eng. **50**, 375 (2003).

8. A. D. Klose and A. H. Hielscher, Med. Phys. **26**, 1698 (1999).
9. A. H. Hielscher, A. Klose, A. K. Scheel, et al., Phys. Med. Biol. **49**, 1147 (2004).
10. A. K. Scheel, M. Backhaus, A. D. Klose, et al., Ann. Rheum. Dis. **64**, 239 (2005).
11. J. B. Fishkin and E. Gratton, M. J. VandeVen, and W. W. Mantulin, Proc. SPIE, **1431**, 122 (1991).
12. S. R. Arridge and W. R. B. Lionheart, Optics Lett. **23** (11), 882 (1998).
13. S. R. Arridge, Inverse Probl. **15**, R41 (1999).
14. D. A. Boas, M. A. O'Leary, B. Chance, and A. G. Yodh, Appl. Opt. **36**, 75 (1997).
15. J. B. Fishkin and E. Gratton, J. Opt. Soc. Am. **10**, 127 (1993).
16. H. Wabnitz and H. Rinneberg, Appl. Opt. **36**, 64 (1997).
17. J. Beuthan, V. Prapavat, R. Naber, et al., Proc. SPIE **2676**, 43 (1996).
18. I. Mesecke-von Rheinbaben, A. Roggan, J. Helfman, et al., Proc. SPIE, **3601**, 482 (1999).
19. J. B. Fishkin, S. Fantini, M. J. VandeVen, and E. Gratton, Phys. Rev. E **53**, 2307 (1996).
20. V. Toronov, E. D'Amico, D. Hueber, et al., Opt. Express **11**, 2717 (2003).
21. B. J. Tromberg, L. O. Svaasand, T. T. Tsay, and R. C. Haskell, Appl. Opt. **32**, 607 (1993).
22. U. Sukowski, F. Schubert, D. Grosenick, and H. Rinnberg, Proc. SPIE **2626**, 92 (1995).
23. A. Roggan, O. Minet, C. Schrunder, and G. Müller, in *Medical Optical Tomography: Functional Imaging and Monitoring*, Ed. by G. Müller, B. Chance, R. Alfano, et al. (SPIE, Bellingham, Washington, 1993), p. 149.